

Inductively coupled plasma etching of deep photonic crystal holes in InP using Cl₂

C.F. Carlström^{a,b}, R. van der Heijden^{a,b}, A.A.M. Kok^a, R.W. van der Heijden^{a,b}, F. Karouta^a, J.J.G.M. van der Tol^a, R. Nötzel^{a,b}, P.J. van Veldhoven^{a,b} and H.W.M. Salemink^{a,b,c}

^aCOBRA Inter-University Research Institute, Eindhoven University of Technology, PO Box 513, NL 5600 MB Eindhoven, The Netherlands

^bCenter for NanoMaterials, Eindhoven University of Technology, PO Box 513, NL 5600 MB Eindhoven, The Netherlands

^cKavli Institute of Nanoscience, Delft University of Technology, P.O. Box 5053, 2600 GB Delft, The Netherlands

We have investigated ICP-etching of deep photonic crystal holes in InP using solely Cl₂ as supplied etching gas. The influence of process parameters on hole geometry is discussed and optical test results are reported.

InP based two-dimensional (2D) deeply etched hole-type photonic crystals are likely to be present in many of the future optical devices involving the telecommunication wavelength of 1550 nm. For operation around 1550 nm a triangular lattice of etched holes with a lattice constant a of ~400 nm and a diameter d of ~250 nm can be used. To fulfill the requirement of low optical loss, the holes should be etched through an InP/InGaAsP/InP planar waveguide structure with a depth of ~2.5 μm and with smooth and vertical sidewalls. (1) Deep photonic crystal holes in InP have been successfully etched using chemically assisted ion beam etching and electron cyclotron resonance reactive ion etching, all based on Cl₂-chemistry. (2,3,4) A versatile etching technique for large-scale fabrication is inductively coupled plasma (ICP) etching, however, so far only one ICP process has been reported for deep hole etching, based on SiCl₄. (5) ICP etching of InP using Cl₂ as main etch gas has been used in other photonic crystal applications such as pillars and shallow holes for membranes. (6, 7) In this work we investigate ICP-etching for fabrication of deeply etched hole-type photonic crystals in the InP-based material system using gas flow consisting solely of Cl₂.

All experiments were performed on (100) n-type Sn-doped InP substrates with a size of approximately 8x8 mm². For optical experiments a waveguide structure consisting of 500 nm InGaAsP ($\lambda=1.25$ μm) with a 500 nm InP upper cladding on top, grown lattice matched to the InP by metal organic vapour phase epitaxy, was used. The photonic crystal pattern is defined into a layer of ZEP520A (positive e-beam resist) with e-beam lithography. This pattern is then transferred into a 400 nm thick, PECVD deposited Si_xN_y-masking layer with a CHF₃-based RIE process. The ICP etch experiments were carried out in a load-locked Oxford Plasmalab 100 system. Since the main etch-product, InCl₃, is not enough volatile at room temperature the etching was performed at elevated temperature. Sample temperature control in ICP etching can be difficult due to significant heating by the ion bombardment. (8) To keep the sample temperature as close to the preset value as possible the

following measures were taken. The samples were glued with heat conducting paste onto a 4 in. silicon carrier wafer. The table temperature was regulated by resistive heating in combination with short sequenced processing (etch steps of 30 s). The stage temperature was measured with a thermocouple. The ion energy was controlled by the negative DC-bias voltage, which is induced by capacitive coupling of additional rf-power to the plasma. Hereby, the relatively low plasma potential is neglected. The chlorine flow was kept constant at 7 sccm. After the ICP etch step the samples were cleaved and the cross-section was inspected with a scanning electron microscope (SEM).

The temperature dependence of the ICP process was investigated for three different ICP/DC-bias combinations at a pressure of 2 mTorr: 250 W/ 640 V, 500 W/ 530 V and 1000 W/ 230 V. An Arrhenius plot of the large area etch rate of the 500 W/ 530 V process is displayed in fig. 1a. A thermally activated etch rate with activation energy of 0.18 eV is observed with the stage temperature fixed between 60 and 200 °C. For higher temperatures the etch rate saturates due to limited supply of chlorine. The other two plasma conditions also exhibit thermally activated etch rate (not shown), however, the activation energy is different, being 0.32 eV at 250 W/ 640 V and 0.10 eV at 1000 W/ 230 V, respectively. The relation between activation energy and ion energy (~DC-bias) points towards a strong influence by the ICP power. Plasma diagnostic such as Langmuir-probe measurements and mass spectroscopy is required to distinguish the role of ion energy, ion current density and plasma composition on surface activation.

Fig. 1b shows the dependence of etch depth on aspect ratio, often denoted as "RIE lag", and the impact of temperature for the 1000 W/ 230 V -process. It should be noted that the etching behavior for holes with diameters \ll 1 μm is strikingly different from that for the large area. The temperature dependence of the lag suggests neutral shadowing or depletion of neutrals as the primary cause of the RIE-lag in our process. (9) Fig. 2 shows the hole shapes of the 200 nm holes etched at different temperatures using the process of fig. 1b.

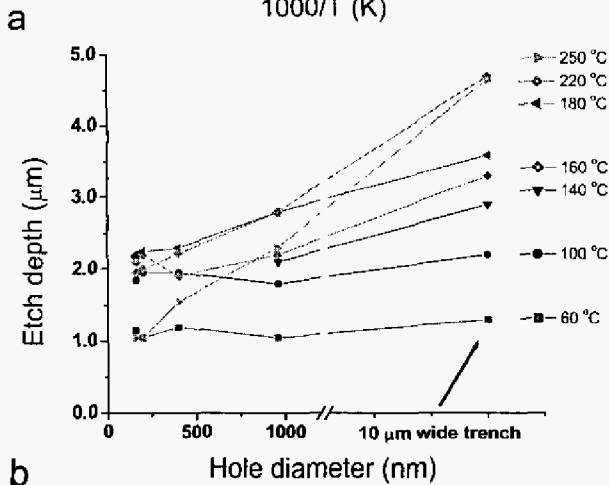
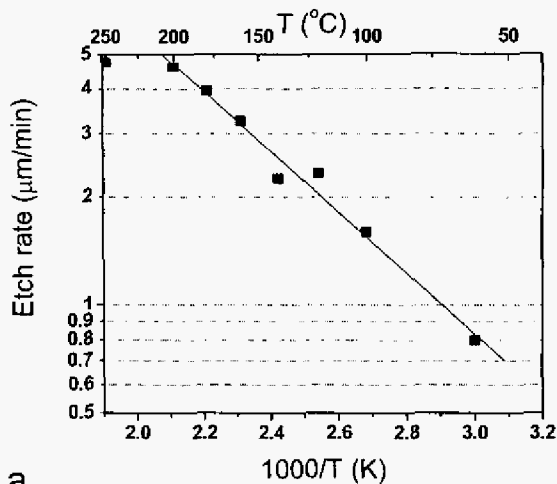


Figure 1: Temperature dependence of (a) the large area etch rate etched at 2mTorr using an ICP power and DC-bias of 500 W and 530 V, and (b) the feature size dependent etch depth for the chlorine process etched for 1 min at 2mTorr using an ICP power and DC-bias of 1000 W and 230 V.

At 160 °C (fig. 2a) the sidewall is tapered with bowing in the upper part indicating that physical etching is significant. (10) When the temperature is increased to 220 °C (fig. 2b) the middle part of the holes becomes more cylinder-like with a distinct tapering only in the lowest part. The under etch in upper region is larger than at 160 °C. In contrast, at 250 °C (fig. 2c) the lowest part of the holes is cylinder-like with flat bottom, while the under etch in the top region is so severe that break down in the sidewall to the neighboring holes can be observed. Interestingly, in the last case the hole depth is smaller (1.1 μm) than at 160 °C (2.2 μm) and 220 °C (1.9 μm). This in combination with the larger under-etch indicates that at high temperatures neutrals are consumed in the upper region and therefore are less available for etching in the lower region. In this case the higher temperature and the ion bombardment provide enough activation of the bottom surface for Cl to form volatile etch products (Cl-flux limited regime).

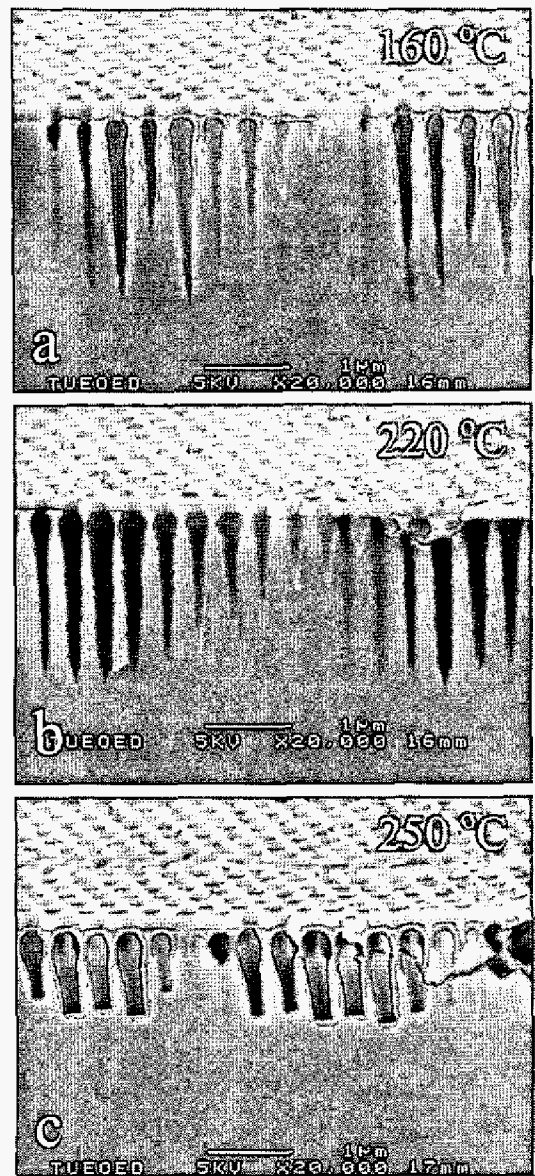


Figure 2: SEM-pictures of a photonic crystal structure with $a = 400$ nm and $d = 200$ nm as etched at (a) 160 °C, (b) 220 °C and (c) 250 °C, respectively. The structures were etched at 2 mTorr using an ICP power and DC-bias of 1000 W and 230 V, respectively. Note that the photonic crystal symmetry axis (ΓK) makes a small angle ($\sim 5^\circ$) with respect to the cleaving plane, giving a 3D impression of the hole-shape. The Si_xN_y mask is left on top.

Therefore any shadow effect of the ion beam due to the high aspect ratio is less important, leading to flat bottom instead of tapered. Similar observations are made for wider holes but the effects are not as marked since the aspect ratio is lower and consequently the Cl-flux is higher. For the other two plasma conditions the observations are consistent with those shown in fig. 2, but the effects are less pronounced when the activation energy is higher.

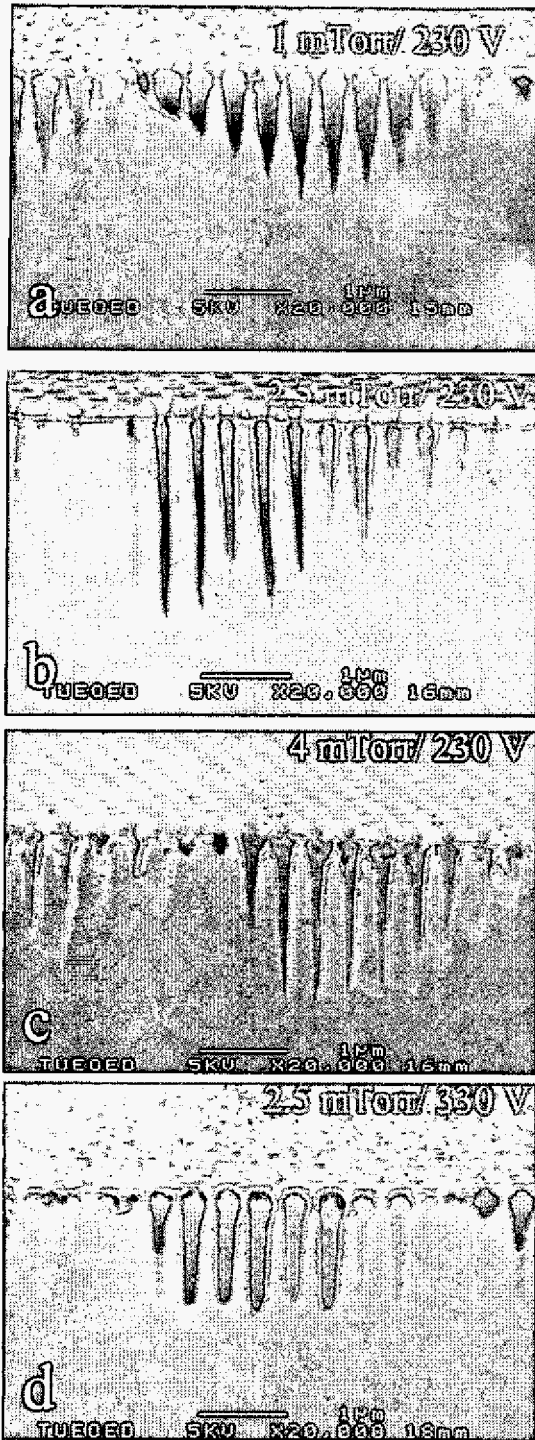


Figure 3: SEM-pictures of a photonic crystal structure with $a = 400 \text{ nm}$ and $d = 200 \text{ nm}$ as etched using (a) 1 mTorr/ 230 V, (b) 2.5 mTorr/ 230 V, (c) 4 mTorr/ 230 V, and (d) 2.5 mTorr/ 330 V, respectively. The temperature was $180 \text{ }^\circ\text{C}$ and ICP power 1000 W. The Si_3N_4 mask is left on top.

To optimize the process for etching of holes the temperature was kept at $180 \text{ }^\circ\text{C}$ as to suppress under etch and maximize the hole depth (see fig. 1b).

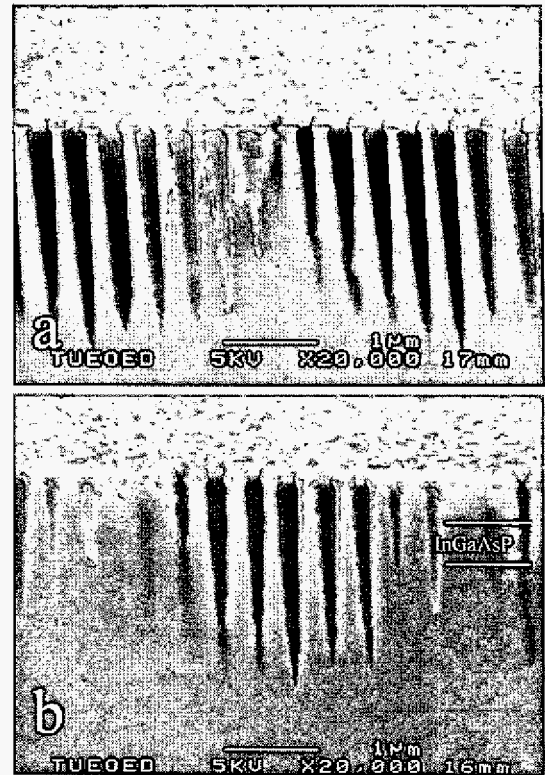


Figure 4: SEM-pictures of a photonic crystal structure with $a = 400 \text{ nm}$ and $d = 200 \text{ nm}$ as etched in (a) InP and (b) InP/InGaAsP/InP, respectively. The structures were etched at $180 \text{ }^\circ\text{C}$ and 2 mTorr using an ICP power and DC-bias of 500 and 530 V, respectively. The Si_3N_4 mask is left on top.

The pressure was varied from 1-4 mTorr for various DC-biases while keeping the ICP power at 1000 W. Fig. 3a-c shows holes with 200 nm diameter etched with 230 V DC-bias at 1, 2.5, and 4 mTorr, respectively. At 1 mTorr (fig. 3a) the lowest region of the holes is tapered while there is severe bowing in the upper region. This bowing may be due to scattering of the ions on the etch mask which appears to be much more eroded than for the higher pressures (fig. 3b-c). Increasing the pressure to 2.5 mTorr (fig. 3b) improves the hole shape, the sidewall being only slightly tapered with a small under etch at the top. The holes are more than 2 μm deep. However, increasing the pressure further to 4 mTorr (fig. 3c) results in a marked under etch in the topmost region, which could derive from the reduced mean free path causing ions to collide in the plasma sheath and hence less anisotropic bombardment. Lower DC-biases (50-150 V) resulted in tapered profiles and in the case of higher pressure (4 mTorr) very little etching (not shown). At higher DC-bias (330 V) the holes are more cylindrical in shape but with large under etch in the top region as can be seen in fig. 3d. This shape resembles that obtained at $220 \text{ }^\circ\text{C}$ with lower DC-bias (fig. 2b) and most likely results from significant heating caused by the ion bombardment. The temperature can be reduced to counter this, but the increased physical bombardment results in poor mask selectivity. Therefore, to etch with higher DC-bias at

180 °C with less heating and mask erosion the ICP power was lowered. The ICP power and DC-bias were varied at 2 mTorr and the best result was obtained using low ICP power (500 W) and high DC-bias (530 V). Fig. 4a shows the cross-section of an InP photonic crystal structure with hole diameter of 200 nm and lattice constant of 400 nm etched under these conditions. The depth is about 2.3 μm with only 250 nm of the Si_xN_y mask consumed during etching. The sidewalls are slightly sloped with a small under etch at the top part. A similar result was obtained for the waveguide structure etched at the same conditions and is shown on fig. 4b. The InGaAsP layer appears as a light contrast and the picture reveals no notable difference in shape to that of InP layers or to the pure InP structure in fig. 4a. These results should be suitable for 2D photonic crystals and a sample with access ridge waveguides in a InP/InGaAsP planar waveguide was prepared.

Optical transmission experiments were carried out on ridge optical waveguides intersected with a 10 period photonic crystal (see insert in fig. 5). The crystal was aligned with respect to the ridge as to measure transmission in the ΓK -direction. The sample was etched under the same conditions as for the structure in fig. 4. To probe the whole stopband, due to the limited bandwidth of the light source (1450-1565 nm) lithographic tuning was employed, using crystals with different lattice constant a and a filling factor of 0.3. (11) The transmission spectra are depicted in fig. 5 and a stopband can be observed. No attempt was made to match the different sections in fig. 5. The mismatches result from the use of different devices on the same sample. As usual, the low frequency bandedge is more pronounced than the high-frequency bandedge. (12) The latter corresponds to the airband where the field is concentrated in the air holes so that losses tend to be higher.

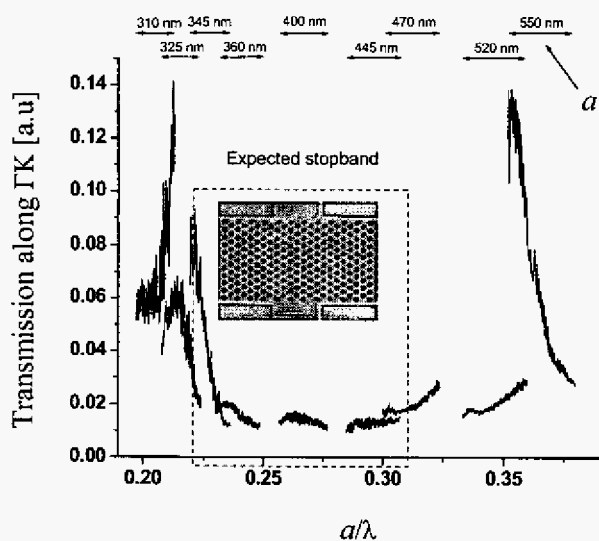


Figure 5: Transmission spectra of the photonic crystals shown in figure 4b along the ΓK direction.

This optical result clearly demonstrates the feasibility of the Cl_2 -ICP process for fabrication of deeply etched hole-type photonic crystals in InP. Further optimization with better hole shape is expected by fine adjusting ICP power, DC-bias, temperature and by addition of sidewall passivation gases. (13)

Acknowledgement

The authors would like to thank E.J. Geluk and P. Nouwens for technical assistance. Part of this research is supported by NanoNed, a technology programme of the Dutch ministry of Economic Affairs.

References

- (1) R. Ferrini, R. Houdré, H. Benisty, M. Qiu, J. Moosburger, *J. Opt. Soc. Am.* B20, 469 (2003).
- (2) M. Mulot, S. Anand, R. Ferrini, B. Wild, R. Houdré, J. Moosburger, A. Forchel, *J. Vac. Sci. Technol.* B22, 707 (2004).
- (3) M.V. Kotlyar, T. Karle, M.D. Settle, L. O'Faolain, T.F. Krauss, *Appl. Phys. Lett.* 84, 3588 (2004).
- (4) T.D. Happ, A. Markard, M. Kamp, A. Forchel, S. Anand, J.L. Gentner, and N. Bouadma, *J. Vac. Sci. Technol.* B19, 2775 (2001).
- (5) F. Pommereau, L. Legouezigou, S. Hubert, S. Sainson, J.P. Chandouineau, S. Fabre, G.H. Duan, B. Lombardet, R. Ferrini, R. Houdre, *J. Appl. Phys.* 95, 2242 (2004).
- (6) H. Hatate, M. Hashimoto, H. Shirakawa, Y. Fujiwara, Y. Takeda, H. Nakano, T. Tatsuta, and O. Tsuji, *Jpn. J. Appl. Phys.* 37(12B), 7172 (1998).
- (7) K. Inoshita, T. Baba, *IEEE J. Selected topics in Quantum Elec* 9(5), 1347 (2003).
- (8) E. Sabin, *J. Vac. Sci. Technol.* B16, 1841 (1998).
- (9) R.A. Gottscho, and C.W. Jurgensen, *J. Vac. Sci. Technol.* B10, 2133 (1992).
- (10) G. Marcos, and A. Rhallabi, *J. Vac. Sci. Technol.* A21, 87 (2002).
- (11) H. Benisty, D. Labilloy, C. Weisbuch, C.J.M. Smith, T.F. Krauss, D. Cassagne, A. Beraud, and C. Jouanin, *Appl. Phys. Lett.* 76, 532 (2000).
- (12) R. Ferrini, D. Leuenberger, M. Mulot, M. Qiu, J. Moosburger, M. Kamp, A. Forchel, S. Anand, and R. Houdre, *J. Quantum. Elec* 38, 786 (2002).
- (13) R. van der Heijden, C.F. Carlström, M.S.P. Andriessse, E. van der Drift, E.J. Geluk, R.W van der Heijden, F. Karouta, P. Nouwens, Y.S. Oei, T. de Vries, and H.W.M. Salemink, *Proceedings Symposium IEEE/LEOS Benelux Chapter, Ghent*, 287 (2004).